BMC Biology

RESEARCH ARTICLE

Open Access

Somatostatin signalling coordinates energy metabolism allocation to reproduction in zebrafish

Jie Chen[1,2], Wenting Zhao[1], Lei Cao[1], Rute S. T. Martins[2] and Adelino V. M. Canário[1,2*]

Abstract

Background Energy allocation between growth and reproduction determines puberty onset and fertility. In mammals, peripheral hormones such as leptin, insulin and ghrelin signal metabolic information to the higher centres controlling gonadotrophin-releasing hormone neurone activity. However, these observations could not be confirmed in lower vertebrates, suggesting that other factors may mediate the energetic trade-off between growth and reproduction. A bioinformatic and experimental study suggested co-regulation of the circadian clock, reproductive axis and growth-regulating genes in zebrafish. While loss-of-function of most of the identified co-regulated genes had no effect or only had mild effects on reproduction, no such information existed about the co-regulated somatostatin, well-known for its actions on growth and metabolism.

Results We show that somatostatin signalling is pivotal in regulating fecundity and metabolism. Knock-out of zebrafish *somatostatin 1.1* (*sst1.1*) and *somatostatin 1.2 (sst1.2)* caused a 20–30% increase in embryonic primordial germ cells, and $sst1.2^{-/-}$ adults laid 40% more eggs than their wild-type siblings. The $sst1.1^{-/-}$ and $sst1.2^{-/-}$ mutants had divergent metabolic phenotypes: the former had 25% more pancreatic α-cells, were hyperglycaemic and glucose intolerant, and had increased adipocyte mass; the latter had 25% more pancreatic β-cells, improved glucose clearance and reduced adipocyte mass.

Conclusions We conclude that somatostatin signalling regulates energy metabolism and fecundity through anti-proliferative and modulatory actions on primordial germ cells, pancreatic insulin and glucagon cells and the hypothalamus. The ancient origin of the somatostatin system suggests it could act as a switch linking metabolism and reproduction across vertebrates. The results raise the possibility of applications in human and animal fertility.

Keywords Trade-off, Fecundity, Metabolism, Diabetes, Zebrafish, Pancreas, Ovary

Background

The activation of the reproductive axis at puberty results from an interplay between hormonal regulation and energy metabolism [1, 2] and understanding the energetic trade-off between growth and reproduction is critical to explain life-history evolution [3]. In mammals, peripheral hormones produced in adipose tissue (leptin), pancreas (insulin) and intestinal tract (ghrelin) signal metabolic information to the higher centres of the hypothalamus-pituitary-gonadal axis (HPG) to activate gonadotrophin-releasing hormone neurones via

*Correspondence:
Adelino V. M. Canário
acanario@ualg.pt
[1] International Research Center for Marine Biosciences, Ministry of Science and Technology and National Demonstration Center for Experimental Fisheries Science Education, Shanghai Ocean University, Shanghai, China
[2] CCMAR/CIMAR Centro de Ciências do Mar do Algarve, Universidade do Algarve, Campus de Gambelas, Faro 8005-139, Portugal

kisspeptins [4, 5]. Insulin can have stimulatory and permissive actions on the HPG partly through leptin stimulation [6, 7]. Ghrelin has direct inhibitory activities on the HPG, and a critical level of leptin needs to be reached in circulation for puberty to proceed and fertility to be maintained [4, 5, 8]. However, although the core function of leptin regulation of appetite appears to be shared between mammals and teleost fish, the primary structure of leptin is poorly conserved and does not seem to be involved in lipid metabolism in fish or to play an essential role in reproduction [9, 10].

In our search for candidates regulating the growth/reproduction metabolic trade-off, we found clock genes *circadian locomotor regulator*, *neuronal PAS domain protein 2*, *basic helix-loop-helix ARNT like 1* and the HPG genes *gonadotrophin-releasing hormone*, *KiSS metastasis suppressor* (*kiss*) and *kiss receptor* share conserved transcription factor frameworks in their promoters in zebrafish, suggesting co-regulation [11]. Additionally, we found co-regulation of the circadian clock and appetite and growth-regulating genes, e.g., *galanin receptor*, *glucagon receptor 1*, *growth hormone receptor* (*ghr*), *leptin*, *agouti signalling protein* and *somatostatin*. Furthermore, experimental photoperiod manipulations and transcriptomics confirmed co-regulation and differential responses of these genes among putative puberal and non-puberal fish [11]. This suggests one or more of these genes as candidates to regulate the metabolic trade-off between and reproduction. Since knockouts and transgenics (from zebrafish, medaka) of most of these gene candidates have normal reproduction or have only mild effects [12–17], we hypothesised somatostatin (SST) as a candidate to regulate the growth-reproduction metabolic trade-off. SST, first discovered in 1973 in sheep hypothalami by Brazeau and Guillemin, regulates growth by inhibiting growth hormone (GH), modulates metabolism by influencing the secretion of pancreatic hormones, and modulates the HPG by inhibiting gonadotrophin-releasing hormone-stimulated luteinising hormone secretion and gonad steroid production [18–21]. Furthermore, in *Drosophila*, allatostatin C, an SST ortholog, induces the secretion of the glucagon-like adipokinetic hormone to coordinate food intake, energy mobilisation, and the progression of oogenesis [22, 23]. However, although SST's growth and metabolism regulation functions appear somewhat conserved [24, 25], a direct role in reproductive function has yet to be demonstrated in vertebrates. To investigate the role of SST in the regulation of metabolism and fecundity, we developed CRISPR/Cas9 zebrafish knockout mutants of *sst1.1* and *sst1.2*, two orthologs of the mammalian *SST1* gene [26, 27] and analysed their metabolic and reproductive phenotype. We found significant metabolic changes associated with pancreatic cell proliferation and fecundity related to germ cell proliferation and metabolic status.

Results

Effect of SST deficiency on growth

Under normal feeding conditions (i.e., feeding twice a day for 10 min), both *sst1.1* and *sst1.2* deficient zebrafish (Additional file: Fig. S1) developed without any visible morphological abnormalities and were slightly longer than their wild type (WT, $sst1.1^{+/+}$) siblings before reaching reproductive maturity, around 55–60 dpf, but not after that stage (Fig. 1a and b; two-way analysis of variance (ANOVA), standard length, *sst1.1* genotype [$F(1,175)= 9.523$, $P=0.002$], age [$F(3,175)= 643.3$, $P<0.001$] and genotype x age [$F(3,175)=3.581$, $P=0.015$]; *sst1.2* genotype [$F(4,256)=390.5$, $P<0.001$] and genotype*age [$F(4,256)=3.044$, $P=0.018$]). The differential growth between WT and SST mutants was not associated with the amount of food consumed, even though the loss of the *sst1.1* gene caused a slightly attenuated appetite (Additional file: Fig. S2).

Effect of SST deficiency on adult fecundity

We compared the $sst1.1^{-/-}$ and $sst1.2^{-/-}$ mutants with their WT siblings at two levels of feeding to determine if there was any effect of genotype on fecundity (i.e., the number of eggs released per clutch) and breeding efficiency (i.e., percentage of successful mating). We found no significant differences in fecundity and breeding efficiency between $sst1.1^{-/-}$ mutants and their WT siblings under normal feeding conditions (Fig. 1c). However, under ad libitum feeding, the breeding efficiency and fecundity increased in the WT but had little effect on the $sst1.1^{-/-}$ mutant. This resulted in 40% lower fecundity and 60% lower breeding efficiency of the $sst1.1^{-/-}$ mutant compared to WT under ad libitum feeding (Fig. 1c; two-way ANOVA, fecundity, effect of genotype [$F(1,92)= 3.975$, $P=0.049$] and feeding level [$F(1,92)= 6.298$, $P=0.014$]; WT $n=44$, $sst1.1^{-/-}$ $n=10$, ad libitum fecundity effect size Cohen's d Hedges correction $g_s =-0.74$, confidence interval CI [−1.44,−0.04]; breeding efficiency, effect of genotype [$F(1,29)= 14.865$, $P<0.001$], feeding level [$F(1,29)= 4.597$, $P=0.014$], interaction genotype*feeding [$F(1,29)=10.190$, $P=0.003$]; ad libitum breeding efficiency effect size WT $n=7$, $sst1.1^{-/-}$ $n=7$, $g_s =-2.44$, CI [−3.82,−1.05]). In contrast, $sst1.2^{-/-}$ mutants had higher fecundity (40% higher for normal feeding and 30% for ad libitum) and breeding efficiency (60% higher for normal feeding and 30% for ad libitum) compared to WT (Fig. 1d; two-way ANOVA, fecundity, effect of genotype [$F(1,217)=19.007$, $P<0.001$] and feeding level [$F(1,217)=45.574$, $P<0.001$]; fecundity normal feeding effect size WT $n=43$, $sst1.2^{-/-}$ $n=80$, $g_s=0.55$, CI

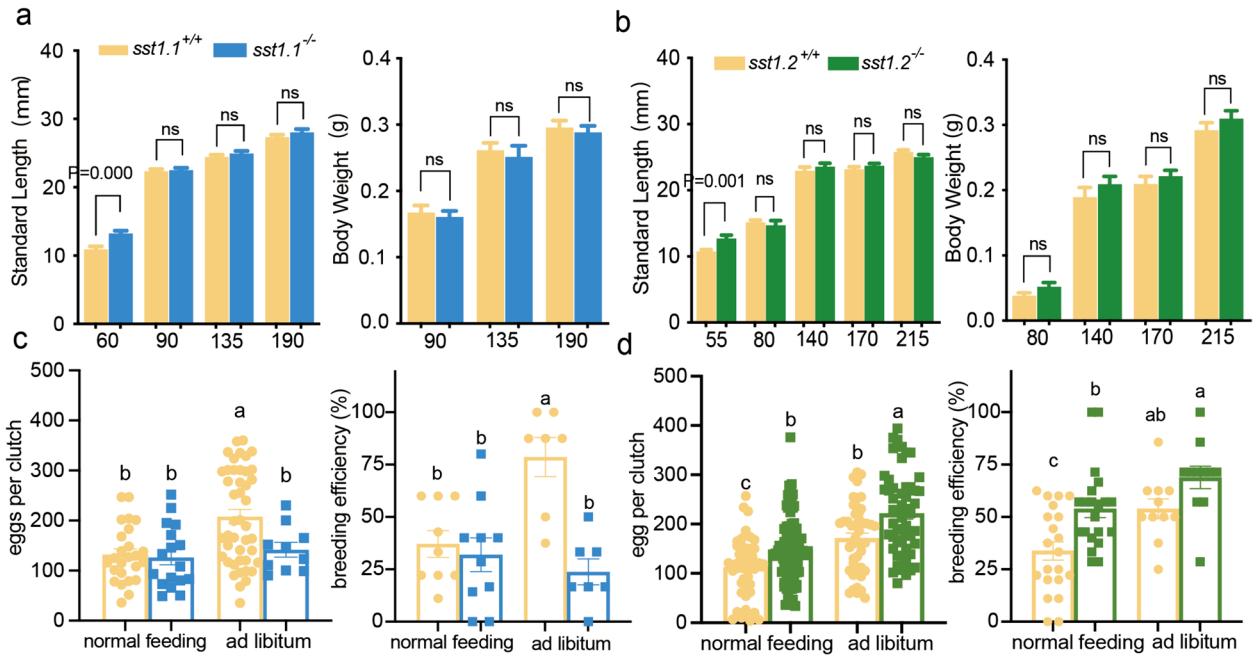

Fig. 1 Growth, fecundity and breeding efficiency of *sst1.1* and *sst1.2* deficient zebrafish and their wild-type siblings. **a** *sst1.1*$^{+/+}$ and *sst1.1*$^{-/-}$ linear and ponderal growth (n=23 to 32 per time point) under normal feeding showing the mutants significantly longer than wild-type only at 60 days. **b** *sst1.2*$^{+/+}$ and *sst1.2*$^{-/-}$ linear and ponderal growth (n=22 to 34 per time point) under normal feeding showing the mutants significantly longer than wild-type only at 55 days. **c** Left, the number of eggs per clutch spawned every 3–5 days by *sst1.1*$^{+/+}$ and *sst1.1*$^{-/-}$ zebrafish under normal and ad libitum feeding, with mutants fed ad libitum spawning significantly fewer eggs than wild type; Right, Breeding efficiency of *sst1.1*$^{+/+}$ and *sst1.1*$^{-/-}$ zebrafish under normal and ad libitum feeding, with mutants fed ad libitum having significantly lower breeding efficiency than wild type. **d** Left, number of eggs per clutch spawned every 3-5 days by *sst1.2*$^{+/+}$ and *sst1.2*$^{-/-}$ zebrafish under normal and ad libitum feeding, with mutants under normal and ad libitum feeding spawning significantly more eggs than wild type; Right, Breeding efficiency under normal and ad libitum feeding with mutants under normal and ad libitum feeding having significantly higher breeding efficiency than wild type. Data are shown as mean ± standard error of the mean

[0.17,0.92]; fecundity ad libitum effect size WT n=46, *sst1.2*$^{-/-}$ n=53, g_s=0.64, CI [0.24,1.05]; two-way ANOVA, breeding efficiency, effect of genotype [F(1,59)=12.040, P<0.001] and feeding level [F(1,59)=12.304, P<0.001]; normal feeding breeding efficiency effect size WT n=21, *sst1.2*$^{-/-}$ n=21, g_s=0.99, CI [0.35,1.63], ad libitum feeding breeding efficiency effect size WT n=11, *sst1.2*$^{-/-}$ n=11, g_s=0.86, CI [−0.01,1.73]).

Effect of SST deficiency on primordial germ cell proliferation

To determine if the hyper-fecundity phenotype observed in *sst1.2*$^{-/-}$ mutants could be related to PGC proliferation, firstly, we performed whole mount in situ hybridisation using a vasa probe in 4 hpf embryos (sphere stage) when germ plasma specification was completed, and four subcellular clumps were formed [28]. We observed that the germ plasma of some of the *sst1.1*$^{-/-}$ and *sst1.2*$^{-/-}$ embryos exhibited smaller and more disorganised (scattered) clumps compared to WT embryos (Additional file: Fig. S3a and b). We observed PGC over-proliferation in the *sst1.1*$^{-/-}$ mutant compared to WT, while *sst1.2*$^{-/-}$ embryos did not show over-proliferation. However, a few individuals seemed to have abundant PGCs (Additional file: Fig. S3). Secondly, we labelled PGCs with *GFP-nos*1 3′UTR capped messenger RNA (mRNA) [29] and utilised laser confocal microscopy to count PGCs in 24 hpf embryos, a time when the PGCs have reached the genital region, completed the initial stage of mitotic proliferation, and their numbers have stabilised [30]. We observed 26.7% over-proliferation of PGCs in *sst1.1*$^{-/-}$ (Fig. 2a) and 41.5% in *sst1.2*$^{-/-}$ (Fig. 2b) embryos compared to WT. The over-proliferation phenotypes were eliminated, and PGC numbers were restored to WT levels when the SST mRNAs were injected to rescue the *sst1.1*$^{-/-}$ (Fig. 2a; one-way ANOVA of effect of genotype and *sst1.1* rescue F(2,43)=17.885, P<0.001; effect size WT n=16, *sst1.1*$^{-/-}$ n=17, g_s=1.20, CI [0.45,1.94]; effect size *sst1.1*$^{-/-}$ n=17, *sst1.1*$^{-/-}$ rescue n=13, g_s =-1.96, CI [−2.84,−1.09]) and *sst1.2*$^{-/-}$ mutants (Fig. 2b; one-way ANOVA of effect of genotype and *sst1.2* rescue F(2,37)= 35.578, P<0.001; effect size WT n= 15, *sst1.2*$^{-/-}$=13 g_s =2.77, CI [1.73,3.81]; effect size *sst1.2*$^{-/-}$ n=13 *sst1.2*$^{-/-}$ rescue n=12, g_s =−2.54, CI [−3.59,−1.49]). Knockdown

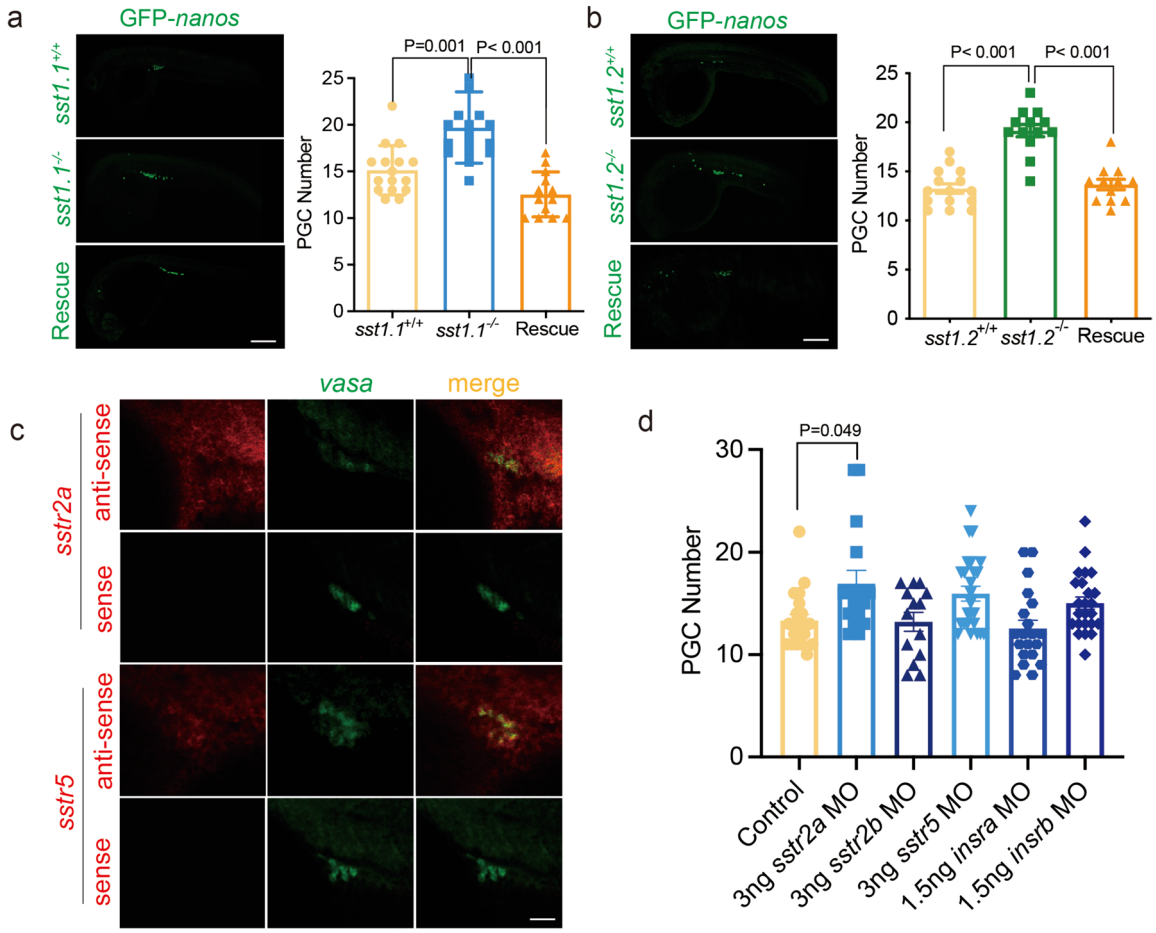

Fig. 2 Visualisation and counting of PGCs in the gonad of 24 hpf zebrafish embryos. **a** Left visualisation of PGCs in embryos injected with *GFP-nos*1 3′UTR capped mRNA in (top) *sst1.1*$^{+/+}$, (middle) *sst1.1*$^{-/-}$, and (bottom) in *sst1.1*$^{-/-}$ rescued by co-injection with *sst1.1* mRNA. Right, histograms show that *sst1.1*$^{-/-}$ developed 26.7% more PGCs than *sst1.1*$^{+/+}$, and the rescue brought PGC numbers down to *sst1.1*$^{+/+}$ levels. **b** Left, visualisation of PGCs in embryos injected with *GFP-nos*1 3′UTR capped mRNA in (top) WT (*sst1.2*$^{+/+}$), (middle) *sst1.2*$^{-/-}$, and (bottom) in *sst1.2*$^{-/-}$ rescued by co-injection with *sst1.2* mRNA. Right, *sst1.2*$^{-/-}$ developed 45% more PGCs than *sst1.2*$^{+/+}$, and the rescue brought PGC numbers down to *sst1.2*$^{+/+}$ level. **c** Fluorescence in situ hybridisation of PGCs showing diffuse expression of *sstr2a* and *sstr5* and their co-expression with vasa in germ cells (column merge). In the bottom panels, RNA sense probes have no staining. **d** Number of PGCs in WT embryos injected with *GFP-nos*1 3′UTR capped mRNA (control) and MO of SST (sstr) or insulin (insr) receptors showing significantly increased PGC numbers only in the *sstr2a*-MO. Data are shown as mean ± standard error of the mean

of *sst1.1* and *sst1.2* using morpholino oligonucleotides (MO) in WT zebrafish replicated the hyper-proliferation phenotype observed in the mutants. However, co-injection of the MO-treated fish with *sst1.1* and *sst1.2* mRNA abolished this phenotype (Additional file: Fig. S4). While our AB strain showed a strong bias towards males, only the *sst1.2*$^{-/-}$ mutant partly reversed this bias (Additional file: Fig. S2).

PGC proliferation is mediated by somatostatin receptor 2a

Next, we aimed to determine the signalling mechanism underlying PGC proliferation mediated by SST. The actions of SST can be either direct through its receptors (SSTR) or indirect through insulin and insulin-like growth factor (IGF) signalling pathways [31]. We first established that *igf2a*, *igf3*, *igf1ra* and *igf1rb* were upregulated compared to WT in the 24 hpf *sst1.2*$^{-/-}$ mutants (Additional file: Fig. S5c, Table S1). To determine if blocking *igf1rb* signalling could reverse the observed PGC over-proliferation, we co-injected *igf1rb*-MO and *GFP-nos*1 3′UTR capped mRNA into one-cell stage *sst1.2*$^{-/-}$ mutants and WT (Additional file: Fig. S5a and b) and found that *igf1rb*-MO caused mis-migration and ectopic localisation of PGC in both *sst1.2*$^{-/-}$ mutants and WT. However, it did not prevent PGC over-proliferation in the *sst1.2*$^{-/-}$ mutants (Additional file: Fig. S5a and b).

We conducted fluorescence in situ hybridisation (FISH) to determine if mRNA for any of the Insr and SSTR co-localised with vasa on the PGCs. Our results revealed *sstr2a* and *sstr5*, but none of the other receptors co-localised with vasa on the PGCs (Fig. 2c; Additional file: Fig. S6). To further investigate the role of these receptors, we injected *sstr2a*-MO and *sstr5*-MO in WT zebrafish to silence the corresponding receptors and counted the number of PGCs in each morphant. We found that silencing *sstr2a* but not *sstr5* replicated the PGC over-proliferation phenotype observed in SST mutants (Fig. 2d; Kruskal-Wallis one-way ANOVA on ranks followed by Dunn's multiple comparisons against WT control H(5)=14.280, P=0.014; effect size of the *sstr2a*-MO n=16, WT control n=16 g_s=0.99, CI [0.25,1.72]). However, experiments using *insra*-MO, *insrb*-MO and *sstr2b*-MO did not show any change in PGC proliferation compared to the WT control (Fig. 2d).

Effect of SST deficiency on carbohydrate and lipid metabolism

To explore possible connections between SST, metabolism and reproduction, we investigated the metabolic characteristics of the SST mutants. Firstly, we measured the glucose levels in 6 dpf larvae (when the yolk sac had been consumed) and adult blood plasma (Figs. 3a and 4a; Additional file: Table S2). We observed that *sst1.1*$^{-/-}$ mutant larvae and adults exhibited hyperglycaemia compared to WT (two-tailed Student's unpaired t-test, n=6 pools of 20 larvae each genotype, effect size g_s =3.83, CI [1.92,5.73]; adults n=17 each genotype, g_s=1.21, CI [0.48,1.94]), whereas *sst1.2*$^{-/-}$ mutant larvae were hypoglycaemic (two-tailed Student's unpaired t-test, n=14 pools of 20 larvae, effect size g_s =−1.24, CI [−2.05,−0.43]) and adult mutants had euglycemic levels. Additionally, *sst1.1*$^{-/-}$ mutants demonstrated poor glucose tolerance and reduced glucose clearance ability (Fig. 3a; two-way ANOVA, effect of glucose treatment F(1,24)=59.166 P<0.001, time F(3,24) P<0.001, glucose × time F(3,24)=3.242 P=0.04, n=4 at each time point, g_s(30 min) =2.14 CI[0.31,3.70], g_s(90 min) =14.04 CI[7.02,21.06], g_s(150 min) =2.85 CI[0.88,4.82]), while *sst1.2*$^{-/-}$ mutants displayed improved glucose tolerance and clearance ability compared to WT (Fig. 4a; two-way ANOVA, effect of glucose treatment F(1,16)=51.497 P<0.001, time F(3,16)= 26.685 P<0.001, glucose × time F(4.797) P=0.014, n=3 at each time point, g_s(30 min)=−5.51 CI[−9.02, −2.01], g_s(90 min) =−2.46 CI[−4.58,−0.34]).

We evaluated the effect of *sst1.1* and *sst1.2* mutations on lipid metabolism by comparing the fluorescent intensity of 28 dpf fish stained with Nile red. We found that the *sst1.1*$^{-/-}$ mutant accumulated more visceral fat than the WT (Fig. 3b; two-tailed Student's unpaired t-test, n=12, g_s =1.43, CI [0.54,2.33]), while the reverse was observed with the *sst1.2*$^{-/-}$ mutant (Fig. 4b; two-tailed Student's unpaired t-test, n=6, g_s =−1.34, CI [−2.59,−0.08]). The *sst1.1*$^{-/-}$ mutant exhibited significantly higher total cholesterol (TC) and triglyceride (TG) than WT in blood plasma after 48 h of fasting (Fig. 3c), whereas the *sst1.2*$^{-/-}$ mutant had lower TC and TG (Fig. 4c; two-tailed Student's unpaired t-test, total cholesterol n=8, g_s =−1.32, CI [−2.40, −0.24], triglyceride t(1%)= −3.783, P=0.002, *sst1.2*$^{-/-}$ n=9, WT n=8 g_s =−1.75, CI [−2.87,−0.63]). Furthermore, both *sst1.1*$^{-/-}$ and *sst1.2*$^{-/-}$ mutant larvae and adult livers showed altered expression of carbohydrate and lipid metabolism genes (Additional file: Fig. S7 and S8, Tables S3 and S4), with the pattern suggesting increased lipid synthesis in the *sst1.1*$^{-/-}$ mutant and more active glucose metabolism and fatty acid oxidation in the *sst1.2*$^{-/-}$ mutant.

We then investigated whether the differences in carbohydrate and lipid metabolism were reflected in alterations in pancreatic glucagon and insulin-producing cells. We crossed each SST mutant with *Tg(gcg:GFP)* [32] and *Tg*(-1.2*ins*:*GFP*) [33] transgenic zebrafish and found that the *sst1.1*$^{-/-}$ mutant had 33% more α-cells than their WT siblings (Fig. 3d) while there was no change in α-cell number in the *sst1.2*$^{-/-}$ mutant (Fig. 4d). Conversely, the *sst1.2*$^{-/-}$ mutant had 30% more β-cells than their WT siblings (Fig. 4e; two-tailed Student's unpaired t-test, t(21)=3.898, *sst1.2*$^{-/-}$ n=11, WT n=12, g_s =1.57 CI [0.63,2.50]), while there was no alteration in β-cell number in the *sst1.1*$^{-/-}$ mutant (Fig. 3e). However, despite the excess of glucagon-producing α-cells, glucagon genes *gcga* and *gcgb* were downregulated (Additional file: Fig. S7). In contrast, insulin genes *insa* and *insb* were upregulated, and *gcga* and *gcgb* were downregulated in the *sst1.2*$^{-/-}$ mutant (Additional file: Fig. S8).

Discussion

This study established SST as a key factor regulating the simultaneous proliferation of primordial germ cells and pancreatic cells and, consequently, fecundity and metabolism in zebrafish. This supports the hypothesis of SST as a critical regulator of the metabolic partition between growth and reproduction.

Under normal feeding conditions, both *sst1.1* and *sst1.2* deficient zebrafish were slightly longer than their wild-type (WT) siblings before reaching reproductive maturity, consistent with the known role of SST in growth regulation [34, 35]. However, this difference disappeared as growth plateaued after they reached sexual maturity, and energy was diverted from growth to reproduction.

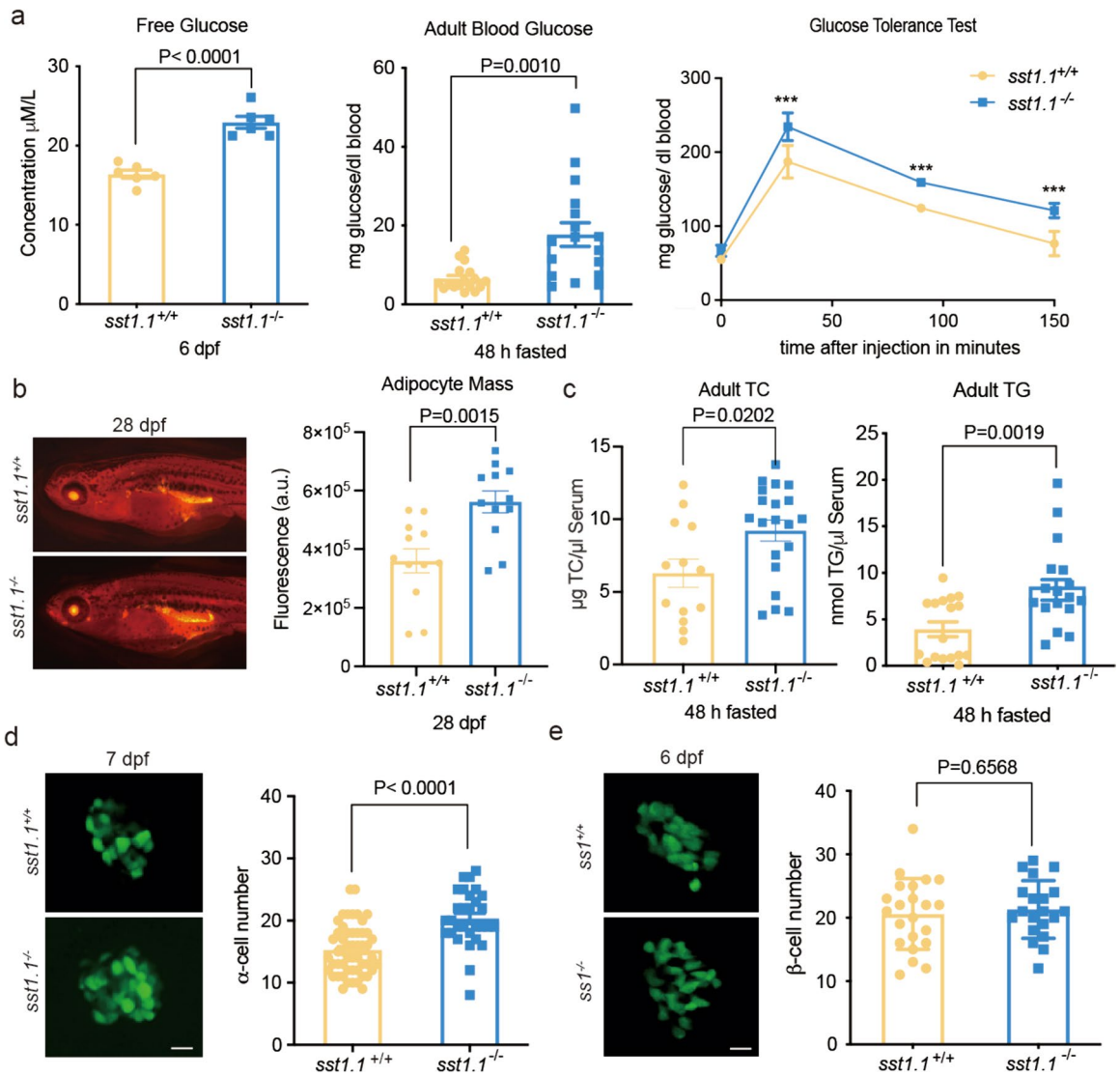

Fig. 3 Metabolic characteristics of the *sst1.1*$^{-/-}$ mutant under normal feeding. **a** The *sst1.1*$^{-/-}$ mutant had higher glucose levels than *sst1.1*$^{+/+}$ in both (left) whole larvae and (centre) adult blood, as well as (right) decreased glucose clearance; Additional file: Table S2; *** $P<0.001$. **b** Left, Nile red staining fluorescence and (right) the corresponding histogram of fluorescence optical density showing the *sst1.1*$^{-/-}$ mutant had more visceral fat than WT. **c** The *sst1.1*$^{-/-}$ mutant had lower blood total cholesterol and higher triglyceride than WT. **d** Crossing the *sst1.1*$^{-/-}$ mutant with a *Tg(gcg:GFP)* zebrafish line allowed (left) visualisation and (right) counting of α-cells to establish that Sst1.1 deficiency caused α-cell proliferation. **e** Crossing the *sst1.1*$^{-/-}$ mutant with a *Tg*(-1.2*ins*:*GFP*) zebrafish line (left) allowed visualisation and (right) counting of β-cells to establish that there was no effect of Sst1.1 deficiency on the β-cell number. Data are shown as mean ± standard error of the mean

Somatostatins regulate adult fecundity

Increasing brine shrimp intake increases fecundity in zebrafish [36], as confirmed in the present study for the two wild-type controls. Interestingly, the *sst1.2*$^{-/-}$ mutant had a significantly increased fecundity and breeding efficiency phenotype compared to the wild-type at the two feeding levels. This contrasted with the *sst1.1*$^{-/-}$ mutant, which had a similar fecundity and breeding efficiency to the wild-type at normal feeding levels but much lower fecundity and breeding efficiency at ad libitum feeding. Whether SST affected germ cells and fertility in null mice models is unclear since litter size or pregnancy alterations have not been reported [37]. However, an anti-somatostatin vaccine and antagonist in mice increased litter size and pregnancy rate [38]. In contrast, although in SST-immunised ewes, pregnancy rates were also higher, litter size was not affected, and in pigs, neither was affected [39].

The effect of SST deficiency in the two mutants could be observed as early as 4 hpf in the smaller and more

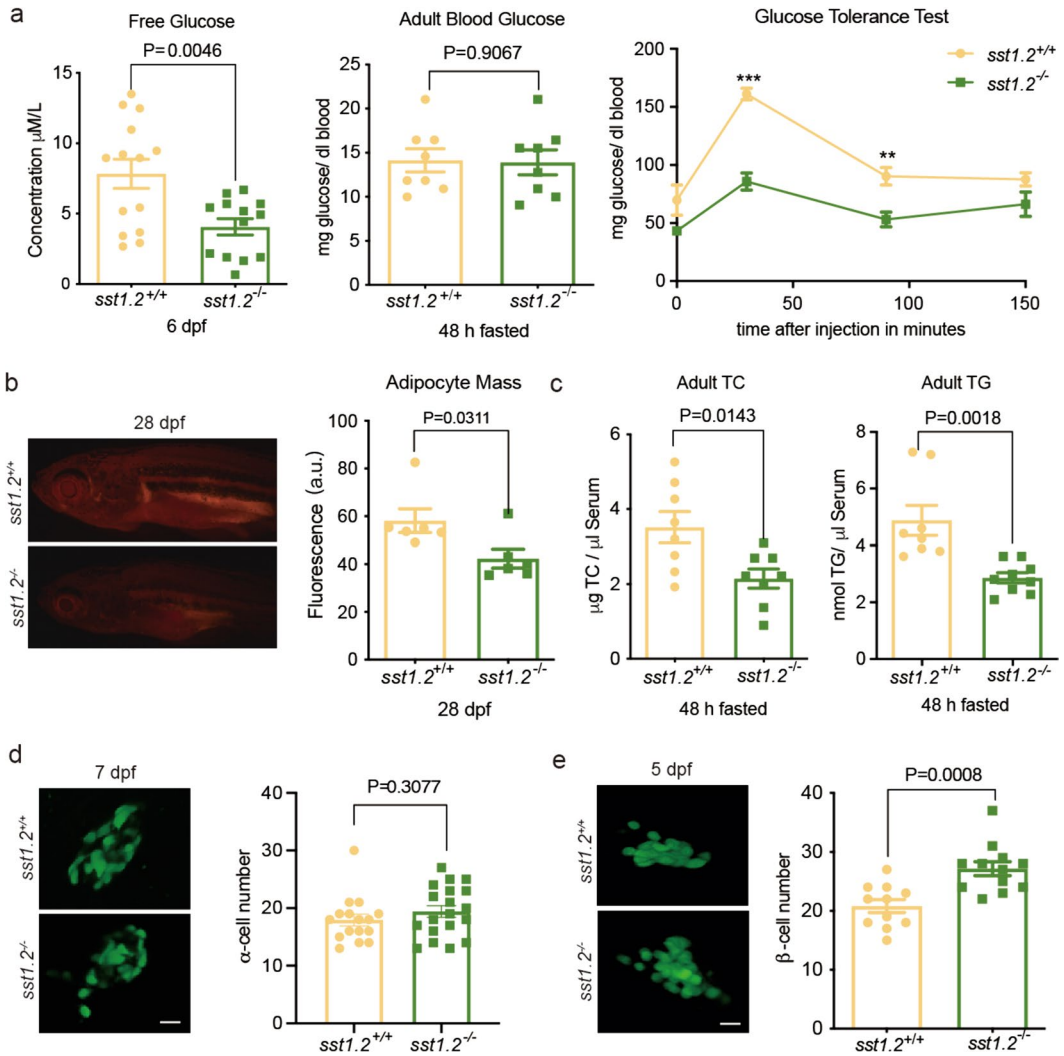

Fig. 4 Metabolic characteristics of the *sst1.2*$^{-/-}$ mutant under normal feeding. **a** Left, the *sst1.2*$^{-/-}$ mutant larvae had lower glucose content than WT, but there were no differences in adult mutant and WT blood glucose. Right, Adult *sst1.2*$^{-/-}$ mutant had greater glucose clearance than WT; Additional file: Table S2, *** $P<0.001$, ** $P<0.01$. **b** Left, Nile red staining fluorescence and (right) the corresponding histogram of fluorescence optical density showing the *sst1.2*$^{-/-}$ mutant had less visceral fat than WT. **c** Left, the *sst1.2*$^{-/-}$ mutant also had lower blood total cholesterol and (right) triglyceride than WT. **d** Left, crossing the *sst1.2*$^{-/-}$ mutant with a *Tg(gcg:GFP)* zebrafish line allowed visualisation and counting of α-cells (right) and established that *sst1.2* deficiency did not affect α-cell proliferation. **e** Crossing the *sst1.2*$^{-/-}$ mutant with a *Tg*(-1.2*ins*:*GFP*) zebrafish line allowed (left) visualisation and (right) counting of β-cells to establish that *sst1.2* deficiency caused β-cell proliferation. Data are shown as mean ± standard error of the mean

disorganised PGCs, which could indicate an early start of migration, which usually happens around 5 hpf [40], consistent with the removal of the inhibitory role of SST on cell migration observed in other cell types [31]. At that stage, PGC over-proliferation could be observed in the *sst1.1*$^{-/-}$ mutant embryos, and by 24 hpf, PGC over-proliferation occurred in both *sst1.1*$^{-/-}$ and *sst1.2*$^{-/-}$ embryos could be rescued by injection of the missing SST mRNAs and was confirmed using MO knockdown.

Differences in PGC proliferation are a feature of male and female sex differentiation, with males undergoing germ cell proliferation arrest [41, 42]. While our AB strain showed a bias towards males, a significant reduction in males in the *sst1.2*$^{-/-}$ but not in the *sst1.1*$^{-/-}$ mutant suggests a possible role of somatostatin signalling, with the differences between the gene products of the two paralogs [43]. This contrasts the zebrafish *gnrh3*$^{-/-}$ phenotype, which exhibited reduced PGC numbers and increased masculinisation [44], suggesting SST and Gnrh3 could work in concert to regulate PGC numbers. However, unlike our *sst1.2*$^{-/-}$ mutant, the reduced PGC phenotype observed in *gnrh3*$^{-/-}$ mutants at 24 hpf

appears transient, as adults exhibited average fecundity [44, 45]. Other factors shown to regulate germ cell number (but not fecundity) include Dead end, which is required for PGC migration and survival [46], and anti-mullerian hormone/anti-mullerian hormone receptor II, which mutations result in excessive germ cell proliferation, premature meiosis in males homozygotes, hypertrophic ovaries and arrested follicular development in female homozygotes leading to lower fertility [47–50].

PGC proliferation is mediated by somatostatin receptor 2a

The actions of SST on PGC proliferation and migration can be either direct through its receptors (SSTR) or indirect through insulin and insulin-like growth factor (IGF) signalling pathways [31]. Knocking down any of the insulin receptors, *insra* and *insrb*, co-expressed with vasa, did not affect PGC numbers, excluding them as possible mediators of PGC proliferation. Although upregulated in the 24 hpf *sst1.2*$^{-/-}$ mutants, *igf2a* and *igf1rb* overexpression or loss-of-function caused PGC mis-migration and ectopic localisation but did not affect their number (as confirmed by our *igf1rb* morpholino), while for *igf1ra* there were no noticeable effects on germ cells [51, 52]. In addition, knockout of *igf3* caused loss of germ cells by apoptosis, but only detectable at 20 dpf [53]. These results indicate that the SST effect on PGC proliferation is independent of Igf signalling.

Of the zebrafish SSTR, only *sstr2a* and *sstr5* co-localised with vasa on the PGCs, and only *sstr2a* silencing replicated the PGC over-proliferation phenotype observed in SST mutants. These findings collectively demonstrate that Sstr2a mediates PGC proliferation regulated by SST. Although we could not find any references in the literature regarding SSTR expression associated with germ cells during early development, SSTR2 and SSTR5 have been reported as the primary mediators of the cell cycle and the anti-proliferative role of SST in other cell types [54], indicating evolutionary conservation of function for these receptors.

Somatostatin regulates carbohydrate and lipid metabolism

The two mutants had a different metabolic profile. Since the preprosomatostatin (pss) produced by the *sst1.1* and *sst1.2* genes yield different peptides, they provide a clue as to the cause of the differential effects. The *sst1.1* pss-I expresses in multiple tissues, including the pancreas [55], and yields a fully conserved SST-14 among vertebrates and the extended peptide SST-26, which can vary in length and sequence with species [43, 56]. The teleost sst1.2 pss-II expresses in the pancreatic islets [55] and contains a not generally secreted SST-14, differing at positions 7 (Tyr for Phe) and 10 (Gly for Thr) of pss-I SST-14, and the secreted peptide encompassing 25 to 28 amino acid residues (28 in zebrafish) [27, 57]. Therefore, the *sst1.1*$^{-/-}$ mutant produces mainly pss-II SST-28, while the *sst1.2*$^{-/-}$ mutant produces mainly pss-I SST-14, which may explain the different phenotypes of the two mutants. In rainbow trout, pss-I and pss-II SST have diverse effects. Injections of salmon pss-I SST-14 and the specific pss-II SST-25 caused hyperglycaemia and increased plasma fatty acid levels and lipase activity while reducing plasma glucagon without affecting insulin levels (SST-14) or reducing both hormones (SST-25) [58, 59]. Neutralisation of SST-25 with antibody decreased lipase activity and elevated insulin levels [60].

The *sst1.1*$^{-/-}$ mutant glucose intolerance phenotype likely results from SST-28 suppressed insulin secretion [61] and high glucagon levels secreted by their larger α-cell mass compensating for the downregulation of glucagon genes resulting from elevated glucose levels [62]. In contrast, the *sst1.2*$^{-/-}$ mutant likely has high insulin levels derived from the upregulation of both the insulin genes (*insa* and *insb*) and an excess of β-cell mass, also resulting in a suppressive effect on α-cells to downregulate *gcga* and *gcgb* [63, 64]. The high insulin and low glucagon levels explain the lipid mobilisation and improved glucose tolerance of the *sst1.2*$^{-/-}$ mutant, and the reverse for *sst1.1*$^{-/-}$ mutant with high visceral fat and plasma lipid and a reduced capacity to tolerate glucose [65].

The phenotypes in our zebrafish mutants differ from the *SST1* deficient mice, which experience loss of α- and β-cell mass [66]. However, the zebrafish phenotypes are consistent with the increased α- and β-cell proliferation after specific ablation of *SST*-expressing δ-cells in mice [67], and with δ-cells contributing to the neogenesis of INS-producing cells during regeneration [68].

Although both mutants produce an excess of germ cells in the embryo, only the adult *sst1.2* deficient mutants were hyper-fecund. This indicates that the two main SST isoforms encoded by *sst1.1* and *sst1.2*, SST-14 and SST-28, have antiproliferative actions on germ cells. Adult fecundity is energy-demanding, and it appears that the *sst1.1*$^{-/-}$ metabolic profile is incompatible with the requirements associated with gametogenesis, as suggested by the decreased fecundity under ad libitum feeding. Previous studies in mice and humans have suggested a possible association between diabetes and lower fecundity [69, 70], suggesting the diabetic phenotype observed in the *sst1.1*$^{-/-}$ mutant may explain its reduced fecundity compared to the wild-type under conditions of increased feeding. In contrast, the hyper-fecund phenotype of the adult *sst1.2*$^{-/-}$ mutant may be due to its more efficient carbohydrate metabolism and lipid mobilisation mediated by SST-14.

The question arises as to how the coordination between metabolism, germ cell proliferation and fecundity may be achieved through SST, in particular since the role of leptin as an adipose mass sensor is not conserved between mammals and fish [9]. SST can have endocrine or paracrine actions and is expressed in multiple tissues, including the zebrafish testis and ovary [55, 71, 72], with inhibitory or stimulatory effects depending on binding to a particular receptor or receptor combinations [73–76]. We speculate that direct and indirect effects of plasma nutrients (e.g., lipids, carbohydrates) on SST secretion [77] could account for tissue-specific effects of SST, including cellular and metabolic effects in the pancreas, germ cell proliferation in the gonads and on the complex regulatory networks that integrate the hypothalamic-pituitary-somatotrophic and HPG axes [78–80]. However, more research is needed to elucidate the specific regulation of the different SST gene products, their effects on target tissues, and the multiple interactions that regulate growth and fecundity.

Conclusions

While it is well established that somatostatins have many functions, often inhibitory and antiproliferative, our findings with *sst1.1* and *sst1.*2 deficient zebrafish demonstrate novel roles regulating PGC proliferation and fecundity, as well as pancreatic α- and β-cells proliferation and metabolism. The *sst1.1* and *sst1.*2 deficient zebrafish phenotypes contrast with the zebrafish knockouts of GnRH, leptin and other genes traditionally associated with reproduction and metabolic sensing that showed mild or no reproductive alterations [9, 44, 45, 81] suggesting somatostatins as candidate key players in the mechanism of energy allocation for growth and reproductive activities. As the *sst1.1/sst1.2* paralogs were already present in the gnathostome ancestor it is likely that these functions are conserved among fishes. However, more studies are needed to understand how the antiproliferative actions of SST are relaxed to allow cell proliferation and interactions with target tissues and other factors to modulate fecundity and energy allocation.

With the loss of the *sst1.2* ortholog in the sarcopterygian/tetrapod lineages [82], and the lack of detailed data on reproductive phenotypes of knockout mice [83], it is not clear whether similar functions are maintained in mammals through the *sst1.1* ortholog. However, the revelation that immunity against SST resulted in larger mice litter sizes [38] suggests potential implications in human fertility treatments, as it may be possible to locally inhibit SST signalling and induce the proliferation of a small number of PGCs and PGC-derived undifferentiated cells with stem cell characteristics found in the human ovary [84]. Additionally, we foresee opportunities to use SST-based technologies in PGC manipulation for animal production and conservation biology.

Methods

Fish general maintenance

Zebrafish of the AB strain were bred and maintained in an Aquatic Habitats Z-Hab aquarium system under controlled conditions. The fish were subjected to a 14-h light and 10-h dark cycle, with a water temperature maintained at 28±0.5°C. Standard zebrafish husbandry practices were followed, including spawning, weaning and maintenance procedures [85]. Mature males and females were paired before the lights were turned off, and the collected embryos were obtained the following morning after the lights were turned on. The developmental stages of the embryos were determined as previously described [86]. The embryos were transferred to Petri dishes with 50 per dish and incubated at 28.5°C for 5 days. After hatching, the larvae were transferred to 1.8-L tanks with manual water renewal and fed *Paramecium* spp twice to thrice daily. Between days 14 and 28, a mixture of *Paramecium* spp. and live *Artemia* spp. was provided as their diet. At 28 days post-fertilisation (dpf), the fish were transferred to 1.8-L tanks and fed live Artemia from that point onward.

Generation of sst1.1 and sst1.2 CRISPR/Cas9 mutants

CRISPR/Cas9 gene-edited zebrafish carrying mutations in exon 1 of the *sst1.1* and *sst1.2* genes were generated as previously described [87]. Sets of specific primers containing the selected target sites (Additional file: Table S5) were used to amplify the genomic regions (GRCz11, sst1.1:chr15:36299017-36300882; *sst1.2*: chr15:36115955-36120277). The gene-specific gRNA was produced by polymerase chain reaction (PCR) amplification of a pUC19-scaffold plasmid (kindly provided by Professor Jingwei Xiong, Peking University) using the target site-specific forward primer and the common reverse primer (additional file: Table S1). The gRNA was synthesised using the MAXIscriptt® T7 in vitro transcription Kit. Cas9 protein (300 pg), purchased from Nanjing Kingsley Biotechnology Co., LTD (Nanjing, China) and gRNA (100 pg) were mixed and injected into the animal pole of zebrafish embryo at 1-cell stage to generate the founders (F0). The founders carrying the mutations were backcrossed with the wild-type zebrafish to generate heterozygous F_1 having 7 bp or 10 bp gene deletions in the case of *sst1.1* mutants and 1 bp insertion or 7 bp gene deletion in the case of *sst1.2* mutants. In each case, peptides lacking the somatostatin function were produced: the 10 bp and 7 bp deletions in exon 1 in the $sst1.1^{-/-}$ mutants caused frame-shift mutations and originated 87 and 88 mature peptides. The $sst1.2^{-/-}$ mutants carried a

7-bp deletion or 1-bp insertion, forming truncated peptides of 24 or 25 amino acids (additional file: Fig. S1).

Growth, breeding efficiency and fecundity

To measure length and weight, zebrafish were fasted for 24 h and anaesthetised with tricaine (300 mg/L). The body length (mm) was measured from the anterior-most region of the mouth to the tail end. Fish were quickly blotted with dust-free paper to remove surface moisture and weighed to the nearest 0.01 mg.

To estimate breeding efficiency (% pairs that successfully mated), breeding pairs were established in the afternoon and maintained separated through a partition in the middle of the breeding tank. The partition was removed the following day, and 1 h later, the number of eggs at the bottom of the tank was counted to determine the fecundity (number of eggs spawned).

The fish were fed freshly hatched brine shrimp (*Artemia spp*). For normal feeding, fish were fed twice a day (at 9:00 and 16:00 h) for 15 min. For ad libitum feeding, fish were fed with excess brine shrimp throughout the day (from 9:00 to 17:00) with the aquarium outlet closed to keep the brine shrimp.

Visualising and counting of PGCs

*GFP-nos*1 3′UTR capped mRNA was produced from the linearised plasmid pCS2pf-*nos*1 3′UTR (provided by Prof. Mingyou Li, Shanghai Ocean University) using the mMessage Machine kit (Ambion, USA) and stored at −80 °C until use. One-cell stage embryos from both wild-type and homozygous mutant zebrafish produced by incrossing the F2 generation were used for the experiments. Embryos were injected with 100 ng of *GFP-nos*1 3′UTR capped mRNA. To facilitate the PGC counting, embryos were depigmented by immersion in 0.225% w/v phenylthiourea (PTU) between approximately 8 and 10 hpf. At 24 hpf, image stacks consisting of 50 slices were acquired at 488 nm excitation from the lateral side of the embryo using a ×10 lens on the Leica TCS SP8 confocal microscope (Leica Microsystems, Germany). The PGCs, identified by their GFP-positive nuclei, were manually counted.

Visualising and counting of pancreatic α- and β-cells

To visualise and count α- and β-cells, transgenic zebrafish lines *Tg*(*ins:GFP*) [33] and *Tg*(*gcga:GFP*) [32] expressing GFP were obtained from the China Zebrafish Resource Center in Wuhan, China. These lines were crossed with the mutant lines generated in this study. The F_1 heterozygous offspring were then incrossed, and the resulting F_2 embryos carrying GFP fluorescence were incubated until 5 days post-fertilisation (dpf) for β-cell analysis and 7 dpf for α-cell analysis.

The larvae were deeply anesthetised and briefly fixed in 4% paraformaldehyde. They were then washed with 1x PBST (phosphate-buffered saline with 0.1% Tween-20) and flat-mounted in Aqua-Mount (Fisher Scientific). The larvae were oriented with their right side facing the coverslip. The larvae were flattened to a sufficient extent to slightly disrupt the islets while allowing for precise resolution of individual cell nuclei.

Using the Leica TCS SP8 confocal microscope, GFP-positive nuclei were manually counted under 488 nm excitation using a ×20 objective. To avoid any observation bias, the genotyping of the fish was performed only after the cell counting procedure was completed.

Morpholino antisense oligonucleotides and rescue mRNA

The morpholino antisense oligonucleotides (Additional file: Table S6) were synthesised by Genetools LLC (OR, USA). One-cell stage WT embryos were co-injected (1 nL) with MO and GFP-nos1 3′UTR capped mRNA (100 ng). The following optimised concentrations of MO were used to ensure normal zebrafish development: 3 ng *sst1.1*-MO; 3 ng sst1.2-MO; 3 ng *sstr2a*-MO; 3 ng *sstr5*-MO; 3 ng *sstr2b*-MO; 1.5 ng *insra*-MO; 1.5 ng *insrb*-MO; 2.5 ng *igf1rb*-MO. The *insra*-MO and *insrb*-MO were previously used by Toyoshima et al. [88], and the *igf1rb*-MO by Schlueter et al. [89]. The control group was injected with the zebrafish standard-MO control.

To rescue the mutant phenotypes, *sst1.1* or *sst1.2* mRNA was co-injected with *GFP-nos*1 3′UTR capped mRNA (100 ng) into mutant and WT siblings (control) one-cell stage embryos. To synthesise *sst1.1* or *sst1.2* mRNA, the *sst1.1* and *sst1.2* coding regions were amplified by RT-PCR and cloned into pGEMT (Promega, USA). The oriented inserts were amplified by RT-PCR, capped with the mMessage Machine kit (Ambion, USA), the poly(A) tail added with the Poly(A) Tailing kit (Invitrogen, Thermo Fisher Scientific, USA) followed by storage at −80 °C until use.

Whole mount and fluorescence in situ hybridisation

Whole-mount in situ hybridisation (ISH) was performed in zebrafish embryos using either digoxigenin (DIG, Roche - Fisher Scientific) or fluorescein isothiocyanate (FITC) labelled probes for vasa, as well as DIG-labelled fluorescence in situ hybridisation (FISH) for the somatostatin and insulin receptors. The protocols were based on previously published methods [90, 91]. Embryos were fixed in 4% paraformaldehyde at 4 °C overnight and dehydrated with an alcohol gradient. After treatment with proteinase K, the embryos were pre-incubated for 4 h at 65 °C. The probes labelled with DIG, or DIG and FITC, were added into the buffer and incubated at 65 °C for at least 16 h.

For ISH, after washing to remove excess probes, samples were incubated with phosphatase-conjugated antibody against DIG at 4 °C overnight and developed in nitro blue tetrazolium/5-bromo-4-chloro-3-indolyl-phosphate (NBT/BCIP, Roche - Fisher Scientific). After staining, embryos were transferred into 3% methylcellulose (Sigma Aldrich) and photographed using an Imager A1 microscope (Zeiss) equipped with a digital camera (AxioCam MRc 5, Zeiss).

For FISH, after washing the excess probes, samples were incubated with an anti-FLU POD antibody (Roche-Fisher Scientific) and stained with the TSA® plus fluorescein kit solution (Perkin Elmer). Samples were then incubated with an anti-DIG POD (Roche-Fisher Scientific) and stained using the TSA Plus Cy3 solution. After staining, embryos were transferred into 1% low melting point agarose and photographed using a Leica TCS SP8 confocal microscope.

Nile Red staining

Nile red (Invitrogen, Fisher Scientific) stain was dissolved in acetone, added to the rearing tank water (0.5 µg/ mL) and left in the dark for 30 min. The dyed zebrafish were anesthetised with tricaine (300 mg/L) and photographed with a Zeiss stereo microscope, and the fluorescence density was analysed with ImageJ image analysis software [92].

Free glucose and glucose tolerance test

Adult zebrafish were anesthetised with ice-cold water, as chemical anaesthetics can interfere with measurements [93]. The tail was severed to obtain a blood sample using a heparinised capillary tube. D-glucose was measured with the Amplex Red glucose assay kit (Invitrogen-Thermofisher Scientific) after diluting the samples 1/100, according to the manufacturer's protocol and measuring the absorbance at 560 nm on a microplate reader. For whole body measurements, pools of 15-20 zebrafish fry were anesthetised with ice-cold water. They were placed into 150 µL 1x reaction buffer, homogenised, kept on ice for 2 h and centrifuged for 10 min at 2500*g* and 4 °C. The glucose levels were measured in the supernatant.

The glucose tolerance test was performed as described by Eames et al. [93]. In the glucose tolerance tests, adult zebrafish were starved overnight and briefly anesthetised with ice-cold water. D-glucose, dissolved in Hanks' buffered salt solution at a concentration of 0.5 mg/g body fish weight, was injected intraperitoneally using a 5-µl micro syringe. Blood samples were collected at 0, 30, 60, 90 and 150 min after injection using a heparinised capillary tube, as described earlier. The fish were anesthetised in ice-cold water, and their tails were severed before blood collection. The collected blood samples were immediately diluted with assay buffer to measure blood glucose levels. Notably, no fish mortalities occurred during the glucose tolerance tests. There were no fish mortalities during the glucose tolerance tests.

Triglycerides and total cholesterol

The blood samples collected for D-glucose measurements were used for triglyceride (TG) and total cholesterol (TC) measurements after dilution 1/100 in 1xPBS. TG was measured using the Triglyceride Quantification Colorimetric Kit and TC with the Total Cholesterol and Cholesteryl Ester Colorimetric Assay Kit (purchased from BioVision, Inc., USA) according to the manufacturer's instructions.

Quantitative reverse transcription polymerase chain reaction

Total RNA was extracted using the Eastep® Super entire RNA extraction kit (Promega, USA) from homogenised pools of 20 fry (6 dpf) or dissected liver fragments from adult zebrafish fish. Nucleic acid quantification and contamination were determined on Nanodrop One (Thermo Scientific). cDNA was synthesised from 1 µg total RNA using the PrimeScript™RT reagent Kit with gDNA Eraser (TaKaRa, Japan) and used to quantify gene expression using primers from the additional file: Table S7 and S8. Quantitative reverse transcription polymerase chain reaction (RT-qPCR) reactions were prepared in a 25 µl reaction volume containing 10 µM forward primer, 10 µM reverse primer and the Faststart Essential Green Master (Roche, Fisher Scientific) according to the manufacturer's protocol and analysed on a LightCycler® 480 (Roche, Fisher Scientific). qPCR specificity was determined by the melting curve method and BLAST of the sequenced amplified fragment. qPCR efficiency was calculated from the slope linear calibration curve and was always >95%. β-actin was used as the internal reference. At least four biological replicates and three technical replicates were used in every case. The no template control was always undetectable. Relative gene expression levels were calculated using the $2^{-\Delta\Delta}$Ct method [94].

Statistics

Comparisons between mutants and wild-type body weight and length at different times, fecundity and breeding efficiency at two feeding levels and glucose clearance over time were analysed by two-way analysis of variance (ANOVA) followed by the Holm-Sidak post hoc test. The effect of morpholinos was analysed by one-way ANOVA followed by the Holm-Sidak. For all other comparisons between each mutant and their wild-type, the two-sided Student's *t* test was used. The Shapiro-Wilk and Brown-Forsythe tests were used to

verify the normality and homogeneity of variances before parametric tests. When the two conditions were not met, the Kruskal-Wallis one-way ANOVA on ranks followed by Dunn's multiple comparisons was used. The effect size was calculated using Hedges' g correction of Cohen's *d* with 95% confidence limits.

Data is presented as mean ± standard error of the mean. Statistical analysis and graphs were done using SigmaPlot v14.0.3.192 (Systat Software Inc., Palo Alto, USA).

Abbreviations

TC	Cholesterol
FISH	Fluorescence in situ hybridisation
GH	Growth hormone
HPG	Hypothalamus-pituitary-gonadal axis
IGF	Insulin-like growth factor
mRNA	Messenger RNA
MO	Morpholino oligonucleotides
PGC	Primordial germ cells
SST	Somatostatin
sst1.2	Somatostatin 1.2
sst1.1	Somatostatin 1.1
SSTR	Somatostatin receptor
TG	Triglyceride
ISH	Whole-mount in situ hybridisation
WT	Wild type

Supplementary Information

The online version contains supplementary material available at https://doi.org/10.1186/s12915-024-01961-7.

Additional file 1: Fig. S1 - Location of target genes in zebrafish chromosomes and generation of CRISPR/Cas9 F0 founders. Fig. S2 – *Artemia nauplii* eaten by zebrafish adults and sex ratios under normal feeding. Fig. S3 – Visualization and counting of PGCs in 4 hpf zebrafish embryos. Fig. S4 – Visualization and counting of PGCs in the gonad of 24 hpf zebrafish embryos treated with *sst1.1* and *sst1.2* morpholinos. Fig. S5 – Effect of insulin-like growth factorsignalling on PGC number and migration in 24 hpf embryos. Fig. S6 – Fluorescence *in situ* hybridisation of PGCs in 24 hpf embryos. Fig. S7 – Expression of endocrine and metabolism-related genes in 6 dpf larvae and in the liver of adults of the $sst1.1^{-/-}$ mutant and $sst1.1^{+/+}$ wild type as measured by qRT-PCR. Fig. S8 – Expression of endocrine and metabolism-related genes in 6 dpf larvae and the liver of adults in the $sst1.2^{-/-}$ mutant and $sst1.2^{+/+}$ wild type as measured by qRT-PCR. Table S1 –Ctdata of the relative difference between the target gene and beta-actin expression for Fig. S5c. Table S2 - Glucose tolerance test data for Figure 3aand Figure 4a. Table S3 - Ctdata of the relative difference between the target gene and beta-actin expression for Fig. S7. Table S4 - Ctdata of the relative difference between the target gene and beta-actin expression for Fig. S8. Table S5 - Primers used in the polymerase chain reaction to amplify the CRISPR/CAS9 gene editing target sequences and to produce the guide RNA. Table S6 - Morpholino antisense sequences. Table S7 - Primer sequences of pancreatic, carbohydrate and lipid metabolism genes used in qPCR. Table S8 - Primer sequences of pancreatic, carbohydrate and lipid metabolism genes used in the quantitative real-time polymerase chain reaction.

Acknowledgements

We thank Prof. Mingyou Li (Shanghai Ocean University) for providing the pCS2pfZf*nos*1 3'UTR plasmid, Prof. Mingyu Li (Xiamen University) for providing the transgenic *Tg(gcga:EGFP)* zebrafish line and the China Zebrafish Resource Centre for providing the transgenic *Tg(-1.2ins:EGFP)* zebrafish line.

Authors' contributions

Conceptualisation: JC, RSTM, AVMC; Methodology: JC, AVMC; Investigation: JC, WZ, LC; Visualisation: JC, AVMC; Funding acquisition: RSTM, AVMC; Project administration: AVMC; Supervision: AVMC; Writing—original draft: JC, RSTM; Writing—review and editing: JC, RSTM, AVMC. All authors read and approved the final manuscript.

Funding

We acknowledge funding from the Shanghai Municipal Government through Shanghai Ocean University and from the Foundation for Science and Technology grants UIDB/04326/2020, UIDP/04326/2020 and LA/P/0101/2020 to AVMC and 2022.08828.PTDC to RSTM.

Availability of data and materials

All data generated or analysed during this study are included in this article and its supplementary information files.

Declarations

Ethics approval and consent to participate

All animal procedures of this research were conducted in compliance with ethical standards and were approved by the Animal Research and Ethics Committee of Shanghai Ocean University under protocol SHOU-DW-2-2020-027.

Consent for publication

Not applicable

Competing interests

The authors declare that they have no competing interests.

Received: 18 September 2023 Accepted: 23 July 2024
Published online: 29 July 2024

References

1. Gerisch B, Weitzel C, Kober-Eisermann C, Rottiers V, Antebi A. A hormonal signaling pathway influencing C. elegans metabolism, reproductive development, and life span. Dev Cell. 2001;1:841–51.
2. Hansen M, Flatt T, Aguilaniu H. Reproduction, fat metabolism, and life span: What is the connection? Cell Metab. 2013;17:10–9.
3. Harshman LG, Zera AJ. The cost of reproduction: the devil in the details. Trends Ecol Evol. 2007;22:80–6.
4. Manfredi-Lozano M, Roa J, Tena-Sempere M. Connecting metabolism and gonadal function: Novel central neuropeptide pathways involved in the metabolic control of puberty and fertility. Front Neuroendocrinol. 2018;48:37–49.
5. Roa J, Tena-Sempere M. Connecting metabolism and reproduction: Roles of central energy sensors and key molecular mediators. Mol Cell Endocrinol. 2014;397:4–14.
6. Bruning JC, Gautam D, Burks DJ, Gillette J, Schubert M, Orban PC, et al. Role of brain insulin receptor in control of body weight and reproduction. Science. 2000;289:2122–5.
7. Pralong FP. Insulin and NPY pathways and the control of GnRH function and puberty onset. Mol Cell Endocrinol. 2010;324:82–6.
8. Casanueva FF, Dieguez C. Neuroendocrine regulation and actions of leptin. Front Neuroendocrinol. 1999;20:317–63.
9. Michel M, Page-McCaw PS, Chen W, Cone RD. Leptin signaling regulates glucose homeostasis, but not adipostasis, in the zebrafish. Proc Natl Acad Sci. 2016;113:3084–9.
10. Parker CG, Cheung E. Metabolic control of teleost reproduction by leptin and its complements: Current insights from mammals. Gen Comp Endocrinol. 2020;:113467.
11. Martins RST, Gomez A, Zanuy S, Carrillo M, Canario AVM. Photoperiodic modulation of circadian clock and reproductive axis gene expression in the pre-pubertal European sea bass brain. Plos One. 2015;10.
12. Hu Z, Ai N, Chen W, Wong QW-L, Ge W. Loss of growth hormone gene (gh1) in zebrafish arrests folliculogenesis in females and delays spermatogenesis in males. Endocrinology. 2019;160:568–86.

13. Tang H, Liu Y, Luo D, Ogawa S, Yin Y, Li S, et al. The kiss/kissr systems are dispensable for zebrafish reproduction: Evidence from gene knockout studies. Endocrinology. 2015;156:589–99.
14. Nakajo M, Kanda S, Karigo T, Takahashi A, Akazome Y, Uenoyama Y, et al. Evolutionally conserved function of kisspeptin neuronal system is nonreproductive regulation as revealed by nonmammalian study. Endocrinology. 2018;159:163–83.
15. Yamashita J, Takeuchi A, Hosono K, Fleming T, Nagahama Y, Okubo K. Male-predominant galanin mediates androgen-dependent aggressive chases in medaka. eLife. 2020;9:e59470.
16. Li M, Dean ED, Zhao L, Nicholson WE, Powers AC, Chen W. Glucagon receptor inactivation leads to α-cell hyperplasia in zebrafish. J Endocrinol. 2015;227:93–103.
17. Ceinos RM, Guillot R, Kelsh RN, Cerdá-Reverter JM, Rotllant J. Pigment patterns in adult fish result from superimposition of two largely independent pigmentation mechanisms. Pigment Cell Melanoma Res. 2015;28:196–209.
18. Heintges T, Lüthen R, Niederau C. Inhibition of exocrine pancreatic secretion by somatostatin and its analogues. Digestion. 1994;55(suppl 1) Suppl. 1:1–9.
19. McCosh RB, Szeligo BM, Bedenbaugh MN, Lopez JA, Hardy SL, Hileman SM, et al. Evidence that endogenous somatostatin inhibits episodic, but not surge, secretion of LH in female sheep. Endocrinology. 2017;158:1827–37.
20. Van Op den bosch J, Adriaensen D, Van Nassauw L, Timmermans J-P. The role(s) of somatostatin, structurally related peptides and somatostatin receptors in the gastrointestinal tract: a review. Regul Pept. 2009;156:1–8.
21. Van Vugt HH, Swarts HJM, Van de Heijning BJM, Van der Beek EM. Centrally applied somatostatin inhibits the estrogen-induced luteinizing hormone surge via hypothalamic gonadotropin-releasing hormone cell activation in female rats. Biol Reprod. 2004;71:813–9.
22. Kubrak O, Koyama T, Ahrentløv N, Jensen L, Malita A, Naseem MT, et al. The gut hormone Allatostatin C/Somatostatin regulates food intake and metabolic homeostasis under nutrient stress. Nat Commun. 2022;13:692.
23. Zhang C, Kim AJ, Rivera-Perez C, Noriega FG, Kim Y-J. The insect somatostatin pathway gates vitellogenesis progression during reproductive maturation and the post-mating response. Nat Commun. 2022;13:969.
24. Canosa LF, Chang JP, Peter RE. Neuroendocrine control of growth hormone in fish. Gen Comp Endocrinol. 2007;151:1–26.
25. Klein SE, Sheridan MA. Somatostatin signaling and the regulation of growth and metabolism in fish. Mol Cell Endocrinol. 2008;286:148–54.
26. Liu Y, Lu D, Zhang Y, Li S, Liu X, Lin H. The evolution of somatostatin in vertebrates. Gene. 2010;463:21–8.
27. Tostivint H, Lihrmann I, Vaudry H. New insight into the molecular evolution of the somatostatin family. Mol Cell Endocrinol. 2008;286:5–17.
28. Yoon C, Kawakami K, Hopkins N. Zebrafish vasa homologue RNA is localized to the cleavage planes of 2- and 4-cell-stage embryos and is expressed in the primordial germ cells. Development. 1997;124:3157–65.
29. Saito T, Fujimoto T, Maegawa S, Inoue K, Tanaka M, Arai K, et al. Visualization of primordial germ cells in vivo using GFP-nos1 3'UTR mRNA. Int J Dev Biol. 2002;50:691–700.
30. Tzung K-W, Goto R, Saju JM, Sreenivasan R, Saito T, Arai K, et al. Early depletion of primordial germ cells in zebrafish promotes testis formation. Stem Cell Rep. 2015;4:61–73.
31. Theodoropoulou M, Stalla GK. Somatostatin receptors: From signaling to clinical practice. Front Neuroendocrinol. 2013;34:228–52.
32. Zecchin E, Filippi A, Biemar F, Tiso N, Pauls S, Ellertsdottir E, et al. Distinct delta and jagged genes control sequential segregation of pancreatic cell types from precursor pools in zebrafish. Dev Biol. 2007;301:192–204.
33. Moro E, Gnügge L, Braghetta P, Bortolussi M, Argenton F. Analysis of beta cell proliferation dynamics in zebrafish. Dev Biol. 2009;332:299–308.
34. Chen W, Ge W. Gonad differentiation and puberty onset in the zebrafish: Evidence for the dependence of puberty onset on body growth but not age in females. Mol Reprod Dev. 2013;80:384–92.
35. Sheridan MA. Coordinate regulation of feeding, metabolism, and growth: Perspectives from studies in fish. Gen Comp Endocrinol. 2021;312: 113873.
36. Newman T, Jhinku N, Meier M, Horsfield J. Dietary intake influences adult fertility and offspring fitness in zebrafish. PLoS One. 2016;11: e0166394.
37. Zeyda T, Hochgeschwender U. Null mutant mouse models of somatostatin and cortistatin, and their receptors. Mol Cell Endocrinol. 2008;286:18–25.
38. Zhang J, Liang A, Bai L, Yang L, Gao J. Effects of a novel recombinant somatostatin DNA vaccination on rat fertility and offspring growth. Afr J Biotechnol. 2012;11:11030–7.
39. Kirkwood RN, Korchinski RS, Thacker PA, Laarveld B. Observations on the influence of active immunization against somatostatin on the reproductive performance of sheep and pigs. J Reprod Immunol. 1990;17:229–38.
40. Paksa A, Raz E. Zebrafish germ cells: motility and guided migration. Curr Opin Cell Biol. 2015;36:80–5.
41. Kurokawa H, Saito D, Nakamura S, Katoh-Fukui Y, Ohta K, Baba T, et al. Germ cells are essential for sexual dimorphism in the medaka gonad. Proc Natl Acad Sci U S A. 2007;104:16958–63.
42. Tong S-K, Hsu H-J, Chung B. Zebrafish monosex population reveals female dominance in sex determination and earliest events of gonad differentiation. Dev Biol. 2010;344:849–56.
43. Tostivint H, Quan FB, Bougerol M, Kenigfest NB, Lihrmann I. Impact of gene/genome duplications on the evolution of the urotensin II and somatostatin families. Gen Comp Endocrinol. 2013;188:110–7.
44. Feng K, Cui X, Song Y, Tao B, Chen J, Wang J, et al. Gnrh3 Regulates PGC proliferation and sex differentiation in developing zebrafish. Endocrinology. 2020;161:1–13.
45. Spicer OS, Wong TT, Zmora N, Zohar Y. Targeted mutagenesis of the hypophysiotropic Gnrh3 in zebrafish (Danio rerio) reveals no effects on reproductive performance. Plos One. 2016;11: e0158141.
46. Weidinger G, Stebler J, Slanchev K, Dumstrei K, Wise C, Lovell-Badge R, et al. dead end, a novel vertebrate germ plasm component, is required for zebrafish primordial germ cell migration and survival. Curr Biol. 2003;13:1429–34.
47. Liu X, Xiao H, Jie M, Dai S, Wu X, Li M, et al. Amh regulate female folliculogenesis and fertility in a dose-dependent manner through Amhr2 in Nile tilapia. Mol Cell Endocrinol. 2020;499: 110593.
48. Zhang Z, Zhu B, Chen W, Ge W. Anti-Müllerian hormone (Amh/amh) plays dual roles in maintaining gonadal homeostasis and gametogenesis in zebrafish. Mol Cell Endocrinol. 2020;517: 110963.
49. Yan Y-L, Batzel P, Titus T, Sydes J, Desvignes T, BreMiller R, et al. A hormone that lost its receptor: Anti-Müllerian hormone (AMH) in zebrafish gonad development and sex determination. Genetics. 2019;213:529–53.
50. Morinaga C, Saito D, Nakamura S, Sasaki T, Asakawa S, Shimizu N, et al. The hotei mutation of medaka in the anti-Müllerian hormone receptor causes the dysregulation of germ cell and sexual development. Proc Natl Acad Sci U S A. 2007;104:9691–6.
51. Sang X, Curran MS, Wood AW. Paracrine insulin-like growth factor signaling influences primordial germ cell migration: In vivo evidence from the zebrafish model. Endocrinology. 2008;149:5035–42.
52. Schlueter PJ, Sang X, Duan C, Wood AW. Insulin-like growth factor receptor 1b is required for zebrafish primordial germ cell migration and survival. Dev Biol. 2007;305:377–87.
53. Xie Y, Huang D, Chu L, Liu Y, Sun X, Li J, et al. Igf3 is essential for ovary differentiation in zebrafish. Biol Reprod. 2021;104:589–601.
54. Buscail L, Estève JP, Saint-Laurent N, Bertrand V, Reisine T, O'Carroll AM, et al. Inhibition of cell proliferation by the somatostatin analogue RC-160 is mediated by somatostatin receptor subtypes SSTR2 and SSTR5 through different mechanisms. Proc Natl Acad Sci. 1995;92:1580–4.
55. Devos N, Deflorian G, Biemar F, Bortolussi M, Martial JA, Peers B, et al. Differential expression of two somatostatin genes during zebrafish embryonic development. Mech Dev. 2002;115:133–7.
56. Plisetskaya EM, Pollock HG, Rouse JB, Hamilton JW, Kimmel JR, Andrews PC, et al. Characterization of coho salmon (Oncorhynchus kisutch) islet somatostatins. Gen Comp Endocrinol. 1986;63:252–63.
57. Conlon JM, Tostivint H, Vaudry H. Somatostatin- and urotensin II-related peptides: Molecular diversity and evolutionary perspectives. Regul Pept. 1997;69:95–103.
58. Eilertson C, Sheridan M. Effects of somatostatin-25 on lipid mobilization from rainbow trout, Oncorhynchus mykiss, liver and adipose tissue incubated in vitro. Comparison with somatostatin-14. J Comp Physiol B. 1994;164:256–60.
59. Eilertson CD, Sheridan MA. Differential effects of somatostatin-14 and somatostatin-25 on carbohydrate and lipid metabolism in rainbow trout Oncorhynchus mykiss. Gen Comp Endocrinol. 1993;92:62–70.

60. Plisetskaya EM, Sheridan MA, Mommsen TP. Metabolic changes in coho and chinook salmon resulting from acute insufficiency in pancreatic hormones. J Exp Zool. 1989;249:158–64.
61. Harmon JS, Eilertson CD, Sheridan MA, Plisetskaya EM. Insulin suppression is associated with hypersomatostatinemia and hyperglucagonemia in glucose-injected rainbow trout. Am J Physiol-Regul Integr Comp Physiol. 1991;261:R609–13.
62. Philippe J. Structure and pancreatic expression of the insulin and glucagon genes. Endocr Rev. 1991;12:252–71.
63. Philippe J. Insulin regulation of the glucagon gene is mediated by an insulin-responsive DNA element. Proc Natl Acad Sci. 1991;88:7224–7.
64. Bansal P, Wang Q. Insulin as a physiological modulator of glucagon secretion. Am J Physiol-Endocrinol Metab. 2008;295:E751–61.
65. Jiang G, Zhang BB. Glucagon and regulation of glucose metabolism. Am J Physiol-Endocrinol Metab. 2003;284:E671–8.
66. Richardson CC, To K, Foot VL, Hauge-Evans AC, Carmignac D, Christie MR. Increased perinatal remodelling of the pancreas in somatostatin-deficient mice: potential role of transforming growth factor-beta signalling in regulating beta cell growth in early life. Horm Metab Res. 2015;47:56–63.
67. Li N, Yang Z, Li Q, Yu Z, Chen X, Li J-C, et al. Ablation of somatostatin cells leads to impaired pancreatic islet function and neonatal death in rodents. Cell Death Dis. 2018;9:1–12.
68. Carril Pardo CA, Massoz L, Dupont MA, Bergemann D, Bourdouxhe J, Lavergne A, et al. A δ-cell subpopulation with a pro-β-cell identity contributes to efficient age-independent recovery in a zebrafish model of diabetes. eLife. 2022;11:e67576.
69. Thong EP, Codner E, Laven JSE, Teede H. Diabetes: a metabolic and reproductive disorder in women. Lancet Diabetes Endocrinol. 2020;8:134–49.
70. Eisenberg ML, Sundaram R, Maisog J, Buck Louis GM. Diabetes, medical comorbidities and couple fecundity. Hum Reprod. 2016;31:2369–76.
71. Patel YC. General Aspects of the Biology and Function of Somatostatin. In: Somatostatin. Berlin, Heidelberg: Springer Berlin Heidelberg; 1992. p. 1–16.
72. Sui C, Chen J, Ma J, Zhao W, Canário AVM, Martins RST. Somatostatin 4 regulates growth and modulates gametogenesis in zebrafish. Aquac Fish. 2019;4:239–46.
73. Ampofo E, Nalbach L, Menger MD, Laschke MW. Regulatory mechanisms of somatostatin expression. Int J Mol Sci. 2020;21:4170.
74. Mandarino L, Stenner D, Blanchard W, Nissen S, Gerich J, Ling N, et al. Selective effects of somatostatin-14, -25 and -28 on in vitro insulin and glucagon secretion. Nature. 1981;291:76–7.
75. Meyerhof W, Wulfsen I, Schonrock C, Fehr S, Richter D. Molecular cloning of a somatostatin-28 receptor and comparison of its expression pattern with that of a somatostatin-14 receptor in rat brain. Proc Natl Acad Sci U A. 1992;89:10267–71.
76. Wang HL, Bogen C, Reisine T, Dichter M. Somatostatin-14 and somatostatin-28 induce opposite effects on potassium currents in rat neocortical neurons. Proc Natl Acad Sci. 1989;86:9616–20.
77. Croze ML, Flisher MF, Guillaume A, Tremblay C, Noguchi GM, Granziera S, et al. Free fatty acid receptor 4 inhibitory signaling in delta cells regulates islet hormone secretion in mice. Mol Metab. 2021;45: 101166.
78. Quintela M, Senaris R, Heiman ML, Casanueva FF, Dieguez C. Leptin inhibits in vitro hypothalamic somatostatin secretion and somatostatin mRNA levels. Endocrinology. 1997;138:5641–4.
79. Watanobe H, Habu S. Leptin regulates growth hormone-releasing factor, somatostatin, and α-melanocyte-stimulating hormone but not neuropeptide Y release in rat hypothalamus in vivo: relation with growth hormone secretion. J Neurosci. 2002;22:6265–71.
80. Stepanyan Z, Kocharyan A, Behrens M, Koebnick C, Pyrski M, Meyerhof W. Somatostatin, a negative-regulator of central leptin action in the rat hypothalamus. J Neurochem. 2007;100:468–78.
81. Trudeau VL. Facing the challenges of neuropeptide gene knockouts: why do they not inhibit reproduction in adult teleost fish? Front Neurosci. 2018;12:302.
82. Tostivint H, Gaillard AL, Mazan S, Pezeron G. Revisiting the evolution of the somatostatin family: Already five genes in the gnathostome ancestor. Gen Comp Endocrinol. 2019;279:139–47.
83. Adams JM, Otero-Corchon V, Hammond GL, Veldhuis JD, Qi N, Low MJ. Somatostatin is essential for the sexual dimorphism of GH secretion, corticosteroid-binding globulin production, and corticosterone levels in mice. Endocrinology. 2015;156:1052–65.
84. De Felici M. Germ stem cells in the mammalian adult ovary: considerations by a fan of the primordial germ cells. Mol Hum Reprod. 2010;16:632–6.
85. Westerfield M. The zebrafish book: a guide for the laboratory use of zebrafish (Danio rerio). 5th edition. Eugene, OR: Printed by the University of Oregon Press : Distributed by the Zebrafish International Resource Center; 2007.
86. Kimmel CB, Ballard WW, Kimmel SR, Ullmann B, Schilling TF. Stages of embryonic development of the zebrafish. Dev Dyn. 1995;203:253–310.
87. Ma J, Chen J, Louro B, Martins RST, Canario AVM. Somatostatin 3 loss of function impairs the innate immune response to intestinal inflammation. Aquac Fish. 2020;6:548–57.
88. Toyoshima Y, Monson C, Duan C, Wu Y, Gao C, Yakar S, et al. The role of insulin receptor signaling in zebrafish embryogenesis. Endocrinology. 2008;149:5996–6005.
89. Schlueter PJ, Royer T, Farah MH, Laser B, Chan SJ, Steiner DF, et al. Gene duplication and functional divergence of the zebrafish insulin-like growth factor 1 receptors. FASEB J. 2006;20:1230–2.
90. Alexander J, Stainier DYR, Yelon D. Screening mosaic F1 females for mutations affecting zebrafish heart induction and patterning. Dev Genet. 1998;22:288–99.
91. Zaidi AU, Enomoto H, Milbrandt J, Roth KA. Dual fluorescent in situ hybridization and immunohistochemical detection with tyramide signal amplification. J Histochem Cytochem. 2000;48:1369–75.
92. Schneider CA, Rasband WS, Eliceiri KW. NIH Image to ImageJ: 25 years of image analysis. Nat Methods. 2012;9:671–5.
93. Eames SC, Philipson LH, Prince VE, Kinkel MD. Blood sugar measurement in zebrafish reveals dynamics of glucose homeostasis. Zebrafish. 2010;7:205–13.
94. Livak KJ, Schmittgen TD. Analysis of relative gene expression data using real-time quantitative PCR and the $2^{-\Delta\Delta C}{}_{T}$ method. Methods. 2001;25:402–8.

Publisher's Note